Journal of Ceramic Processing Research. Vol. 18, No. 7, pp. 543~549 (2017)

J O U R N A L O F
Ceramic Processing Research

Effect of LaPr-Co co-substitution on microstructure and magnetic properties for $Ca_{0.4}Sr_{0.6-x}(La_{0.8}Pr_{0.2})_xFe_{12-y}Co_yO_{19}$ hexaferrites

Yujie Yang*, Mou Wu, Fanhou Wang, Juxiang Shao and Qilong Cao

Computational Physics Key Laboratory of Sichuan Province, School of Physics and Electronic Engineering, Yibin University, Yibin 644007, P. R. China

M-type hexaferrites with nominal composition of $Ca_{0.4}Sr_{0.6-x}(La_{0.8}Pr_{0.2})_xFe_{12-y}Co_yO_{19}$ ($0.00 \le x \le 0.50$, $0.00 \le y \le 0.40$) were prepared by the solid-state reaction method. X-ray diffraction (XRD), field emission scanning electron microscopy (FE-SEM) and a permanent magnetic measuring system were used to investigate the microstructural and magnetic properties of the M-type hexaferrites. All the LaPr-Co substituted M-type hexaferrites are in single-phase with hexagonal structure and no impurity phase is observed in the structure. The FE-SEM images of the magnets show that the grains are hexagonal platelet-like, and the grain size of the magnets basically keeps unchanged with increasing LaPr-Co content. The remanence (B_r), first decreases, and reaches to the minimum value at x = 0.20, y = 0.16, and then increases with the increasing substitution content of LaPr ($0.20 \le x \le 0.50$) and Co ($0.16 \le y \le 0.40$). The intrinsic coercivity (H_{cj}) increases with the increase of LaPr-Co content ($0.00 \le x \le 0.40$, $0.00 \le y \le 0.32$), and then decreases with the increasing substitution content of LaPr ($0.40 \le x \le 0.50$) and Co ($0.32 \le y \le 0.40$). Magnetic induction coercivity (H_{cb}) and maximum energy product [$(BH)_{max}$] increase with increasing LaPr-Co content ($0.00 \le x \le 0.50$, $0.00 \le y \le 0.40$).

Key words: M-type hexaferrites, LaPr-Co co-substitution, X-ray diffraction, Magnetic properties.

Introduction

In 1950s, M-type hexagonal ferrites were discovered by Philips' laboratories [1]. M-type hexaferrites have attracted extensive studies in the past decades because of their chemical stability, moderate magnetic properties, low cost compared to rare earth magnetic materials [1]. M-type hexaferrites have been used as permanent magnets, plastic magnets, microwave devices and magnetic recording media [2].

The magnetic properties of M-type hexaferrites depend on the synthesis conditions and the ion site occupation of the substituted ions in five different Fe^{3+} sublattices, such as three octahedral (2a, 12k and $4f_2$), one bipyramidal (2b) and one tetrahedral ($4f_1$) [3]. The intrinsic magnetic properties of M-type hexaferrites can be modified through the ion substitution of Sr^{2+} or Ba^{2+} ions or Fe^{3+} ions [4, 5]. It has been reported that rare earth metal ions, such as La^{3+}, Pr^{3+}, Dy^{3+}, Nd^{3+}, $Sm^{3+}$and Ce^{3+}, prefer to substitute partly Sr^{2+} or Ba^{2+} ions [4, 6-10], and transition metal ions, such as Co^{2+}, Zn^{2+}, Cu^{2+}, Bi^{3+}, Cr^{3+}, Al^{3+} and Mn^{3+}, prefer to substitute Fe^{3+} ions [5, 11-16]. Liu et al. [4] have prepared the La^{3+} substituted M-type strontium hexaferrites with the composition $Sr_{1-x}La_xFe_{12}O_{19}$ ($0.00 \le x \le 1.00$) by the ceramic process and found that with increasingLa^{3+} substitution, σ_s and H_{ci} first increase and then decrease gradually, while the Curie temperature of $Sr_{1-x}La_xFe_{12}O_{19}$ hexaferrites linearly decreases with the increase of La^{3+} substitution. Wang et al. [6] have synthesized the Pr doped strontium hexaferrites by hydrothermal synthesis and subsequent calcinations and found that Pr substitution increase the coercivity by 14% without causing any significant deterioration in either the magnetization or the remanence. Vizhi et al. [7] have studied the influence of Co substitution on magnetic properties of nanocrystalline $Ba_{0.5}Sr_{0.5}Fe_{12-x}Co_xO_{19}$ (x = 0, 0.5, 0.7 and 0.9), with increasing Co ion content, M_s first increases and then decreases, while H_{ci} decreases with the increase of Co ion content. Yang et al. [15] have synthesized the Al substituted M-type Ca-Sr hexaferrites, with composion $Ca_{0.6}Sr_{0.1}La_{0.3}Fe_{12-x}Al_xO_{19}$ ($0 \le x \le 1.4$) by the conventional ceramic techniques and found that M_s and M_r linearly decrease with x from 0 to 1.4, while H_c first increases with x from 0 to 0.8 and then decreases when $x \ge 0.8$. Ion combination substitutions, such as La^{3+}-Zn^{2+}, La^{3+}-Co^{2+}, La^{3+}-Cu^{2+}, Mn^{2+}-Zn^{2+}, Pr^{3+}-Ni^{3+}, Ce^{3+}-Co^{2+}, Nd^{3+}-Ni^{2+}, and Tb^{3+}-Zn^{2+}, have been reported [17-24]. Yang et al. [18] have prepared the hexagonal ferrite $Sr_{0.7-x}Ca_{0.3}La_xFe_{12-y}Co_yO_{19}$ (x = 0.05-0.50; y = 0.04-0.40) magnetic powders and magnets by the solid state reaction method and found that the remanence continuously increases with increasing La-Co contents, while the magnetic induction coercivity, intrinsic

*Corresponding author:
Tel : +86-831-3531171
Fax: +86-831-3531161
E-mail: loyalty-yyj@163.com

coercivity and maximum energy product for the magnets first increases and then decreases with the increase of La-Co contents. Zi et al. [22] have synthesized the Ce-Co doped M-type barium hexaferrites $Ba_{1-x}Ce_xFe_{12-x}Co_xO_{19}$ ($0.0 \le x \le 0.3$) by the sample chemical coprecipitation method and found that with the increase of Ce-Co content, the saturation magnetization (M_s) decreases monotonically with increasing x, while the coercivity (H_c) increases at low substitution ($x \le 0.1$), and then decreases at $x \ge 0.1$.

In the present work, La^{3+} and Pr^{3+} are selected to dope the Sr^{2+} ions and Co^{2+} ions are selected to dope the Fe^{3+} ions. The solid-state reaction method was used to prepare the LaPr-Co substituted M-type CaSr hexaferrites. We have carefully investigated the influence of LaPr-Co content on the microstructure and magnetic properties of M-type CaSr hexaferrites.

Experimental Procedure

The solid-state reaction method was used to synthesize the M-type hexaferrites with nominal composition of $Ca_{0.4}Sr_{0.6-x}(La_{0.8}Pr_{0.2})_xFe_{12-y}Co_yO_{19}$ (where $x = 0.00$, 0.10, 0.20, 0.30, 0.40, 0.50; $y = 0.00$, 0.08, 0.16, 0.24, 0.32, 0.40). The starting powders of $CaCO_3$, $SrCO_3$, La_2O_3, Pr_6O_{11}, Fe_2O_3 and CoO, all 99% pure, were weighted in accordance with the ratios of the nominal composition. The starting powders were wet-mixed in a ball mill at a rotate speed of 80 rpm for 8 hrs. After that, the mixed powders were dried in a drying oven in the air, and then calcined in a muffle furnace at 1250 °C for 2.0 hrs in air. Next, the calcined powders were shattered to particles by a vibration mill, and then wet-milled with suitable additives (0.6 wt% $CaCO_3$, 0.3 wt % $SrCO_3$, 0.2 wt % SiO_2, 0.2 wt% $Ca(C_6H_{11}O_7)_2$) for 16 hrs in a ball-mill. At the final step, the finely milled slurry was pressed into cylindrical pellets (Φ30 mm × 16 mm) under 310 MPa in the magnetic field of 800 kA/m, which was parallel to the pressing direction. The compacted pellets were sintered in a muffle furnace at 1185 °C for 1.5 hrs in air. In order to measure the magnetic properties, the sintered pellets were polished in the faces perpendicular to the pressing direction.

The phase compositions and structure of the prepared magnetic powders were identified by using a PANalytical X'Pert Pro diffractometer in continuous mode with Cu K_α radiation in the range of $2\theta = 20$-80 °. The images of the surface of the sintered pellets were observed by a HITACHI S-4800 field emission scanning electron microscopy (FE-SEM). A permanent magnetic measuring system (NIM-2000HF, made by the National Institute of Metrology of China) was used to measure the magnetic properties of the sintered pellets at room temperature.

Results and Discussion

Fig. 1 shows the XRD patterns of the M-type hexaferrite $Ca_{0.4}Sr_{0.6-x}(La_{0.8}Pr_{0.2})_xFe_{12-y}Co_yO_{19}$ ($0.00 \le x \le 0.50$, $0.00 \le y \le 0.40$) magnetic powders. All the diffraction peaks are matched with the standard patterns (space group $P6_3/mmc$, JCPDS card no. 80-1198). This reveals that all the LaPr-Co substituted M-type hexaferrites are in single-phase with hexagonal structure and no impurity phase is observed in the structure.

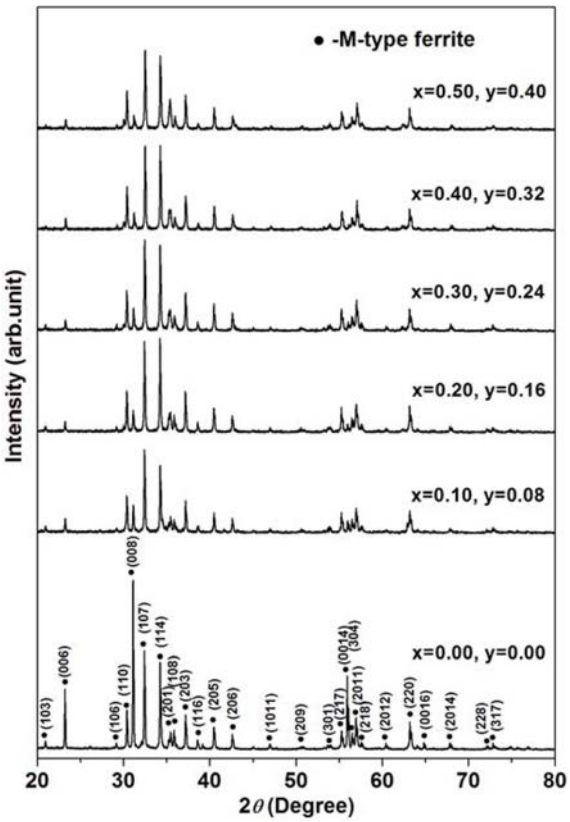

Fig. 1. XRD patterns of the M-type hexaferrite $Ca_{0.4}Sr_{0.6-x}(L_{a0.8}Pr_{0.2})xFe_{12-y}Co_yO_{19}$ ($0.00 \le x \le 0.50$, $0.00 \le y \le 0.40$) magnetic powders.

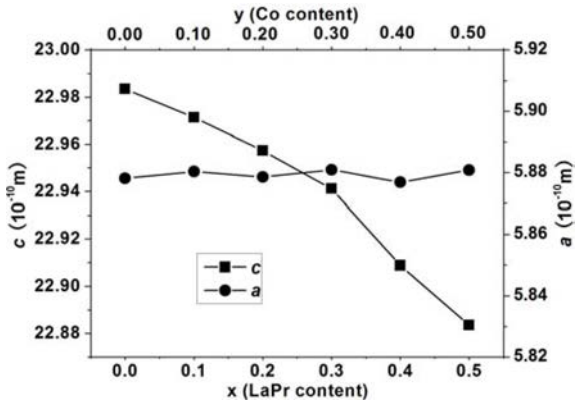

Fig. 2. The variation of lattice constants (c and a) as a function of LaPr-Co content for the M-type hexaferrite $Ca_{0.4}Sr_{0.6-x}(La_{0.8}Pr_{0.2})_xFe_{12-y}Co_yO_{19}$ magnetic powders.

The lattice parameters (c and a) are calculated from the XRD data by using the following relation [25]:

$$\frac{1}{d_{hkl}^2}=\frac{4}{3}\times\frac{h^2+hk+k^2}{a^2}+\frac{l^2}{c^2} \quad (1)$$

where d_{hkl} is the inter-planer spacing value, and h, k and l are the Miller indices. Fig. 2 shows the variation of lattice parameters for as a function of LaPr-Co content for the M-type hexaferrite $Ca_{0.4}Sr_{0.6-x}(La_{0.8}Pr_{0.2})_xFe_{12-y}Co_yO_{19}$ magnetic powders. The lattice parameter a remains almost constant, while the lattice parameter c decreases with the increase of LaPr-Co content. Hexaferrites are anisotropic as c-axis is the easy axis and it is easier to orient the spin directions along c-axis which is perpendicular to the hexagonal based plane [26]. Thus, the variation of lattice parameter c is sizeable rather than lattice parameter a. The decrease of lattice parameter c with the increase of LaPr-Co content can be due to the difference in the ionic radii (Δr) of the metal ions and the number of ionic substitutions of each species. Substitution of Sr^{2+} (r = 1.180 Å) by La^{3+} (r = 1.061 Å) and Pr^{3+} (r = 1.013 Å) makes a negative difference in the ionic radii of Δr = –0.1286 Å. Thus, substitution of Fe^{3+} (r = 0.645 Å) by Co^{2+} (r = 0. 745 Å) makes a positive difference in the ionic radii of Δr = + 0.100 Å. In the LaPr-Co substituted M-type hexaferrites, in order to keep the electroneutrality, some Fe^{3+} ions (r = 0.645 Å) will change into Fe^{2+} ions (r = 0.780 Å) at 2a or $4f_2$ site, this makes a positive difference in the ionic radii of Δr = +0.135 Å. As in the case of substitution of LaPr (x = 0.40) and Co (x = 0.32), the total content of both $Co^{2+}$and Fe^{2+} ions is equal to that of La^{3+} and Pr^{3+} ions, and the lattice parameter c is decreased.

The variation of c/a ratios as a function of LaPr-Co content for the M-type hexaferrite $Ca_{0.4}Sr_{0.6-x}(La_{0.8}Pr_{0.2})_xFe_{12-y}Co_yO_{19}$ magnetic powders is shown in Fig. 3. The c/a ratios of the magnetic powers decrease with the increase of LaPr-Co content. The c/a ratio may be used to quantify the structure type, and an M-type hexagonal structure may be assumed if the ratio is lower than 3.98 [27]. It is seen from Fig. 3 that the c/a ratio is in the range from 3.8912 to 3.9100, which indicates the formation of M-type hexagonal structure.

Fig. 4 shows the representative FE-SEM micrographs of the M-type hexaferrite $Ca_{0.4}Sr_{0.6-x}(La_{0.8}Pr_{0.2})_xFe_{12-y}Co_yO_{19}$ magnets for x = 0.00, y = 0.00; x = 0.20, y = 0.16; x = 0.40, y = 0.32. It is clear that most of the grains have well-defined shape and boundaries. The

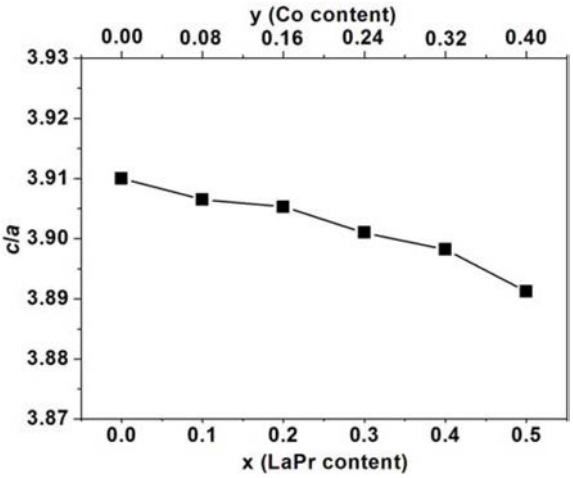

Fig. 3. The variation of c/a ratios as a function of LaPr-Co content for the M-type hexaferrite $Ca_{0.4}Sr_{0.6-x}(La_{0.8}Pr_{0.2})_xFe_{12-y}Co_yO_{19}$ magnetic powders.

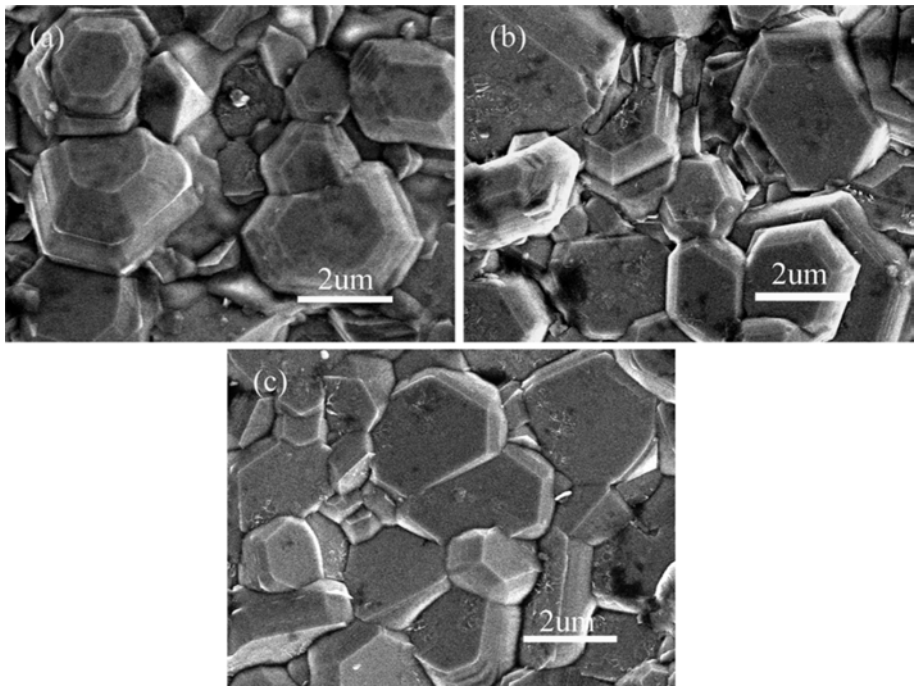

Fig. 4. Representative FE-SEM images of the M-type hexaferrite $Ca_{0.4}Sr_{0.6-x}(La_{0.8}Pr_{0.2})_xFe_{12-y}Co_yO_{19}$ magnets for (a) x = 0.00, y = 0.00; (b) x = 0.20, y = 0.16; (c) x = 0.40, y = 0.32.

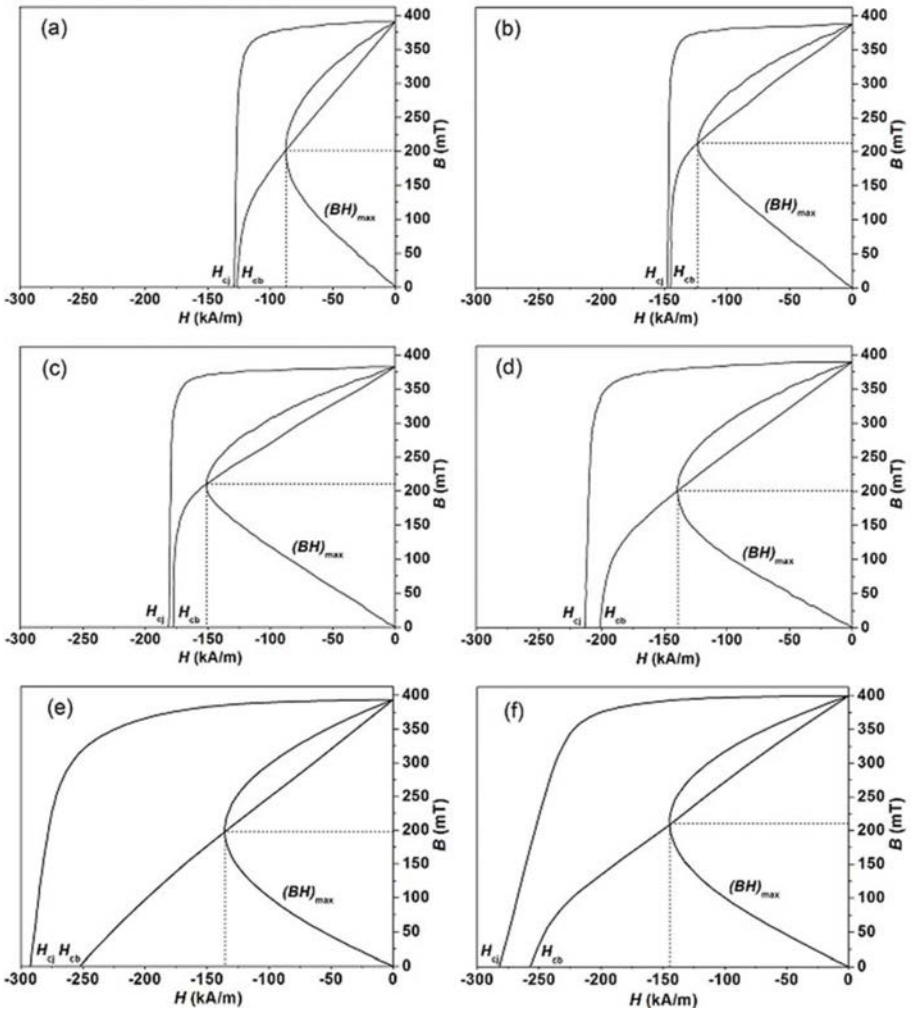

Fig. 5. Demagnetizing curves for the M-type hexaferrite $Ca_{0.4}Sr_{0.6-x}(La_{0.8}Pr_{0.2})_xFe_{12-y}Co_yO_{19}$ ($0.00 \le x \le 0.50$, $0.00 \le y \le 0.40$) magnets measured at room temperature.

grains are hexagonal platelet-like, and the grain size of the magnets basically keeps unchanged with increasing LaPr-Co content.

Fig. 5 shows the demagnetizing curves for the M-type hexaferrite $Ca_{0.4}Sr_{0.6-x}(La_{0.8}Pr_{0.2})_xFe_{12-y}Co_yO_{19}$ ($0.00 \le x \le 0.50$, $0.00 \le y \le 0.40$) magnets measured at room temperature. The values of the remanence (B_r), intrinsic coercivity (H_{cj}), magnetic induction coercivity (H_{cb}) and maximum energy product [$(BH)_{max}$] were calculated from the demagnetizing curves. The variation behavior of the remanence (B_r) of the M-type hexaferrite $Ca_{0.4}Sr_{0.6-x}(La_{0.8}Pr_{0.2})_xFe_{12-y}Co_yO_{19}$ magnets as a function of LaPr-Co content is shown in Fig. 6. With increasing LaPr-Co content, the value of B_r first decreases, and reaches to the minimum value at $x = 0.20$, $y = 0.16$, then increases. In the M-type hexaferrite, the Fe^{3+} ions are distributed on five different interstitial sites: one tetrahedral site $4f_1$ (downward spin), one bipyramidal site 2b (upward spin), three octahedral sites 2a (upward spin), $4f_2$ (downward spin), 12k (upward spin). The magnetic moments of Fe^{3+} ions in the hexagonal ferrite are arranged collinearly because of super-exchange

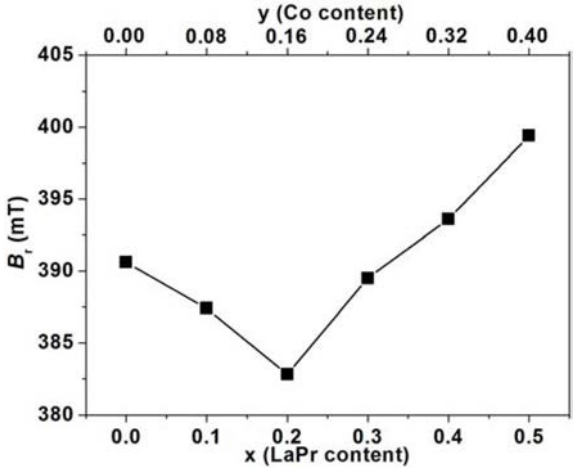

Fig. 6. The variation behavior of the remanence (B_r) of the M-type hexaferrite $Ca_{0.4}Sr_{0.6-x}(La_{0.8}Pr_{0.2})_xFe_{12-y}Co_yO_{19}$ magnets as a function of LaPr-Co content.

interaction. It has been reported that Co^{2+} ions are substituted for Fe^{3+} ions in the octahedral $4f_2$ (mainly)

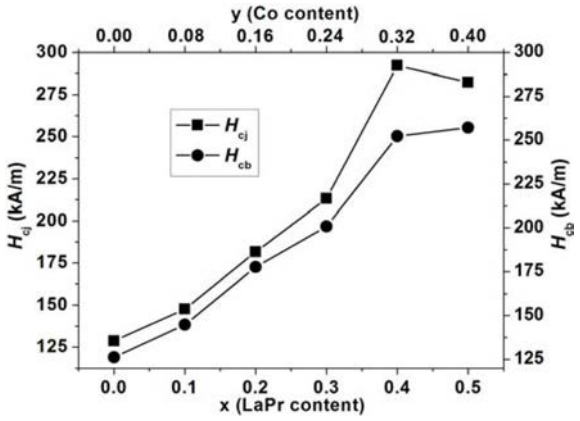

Fig. 7. The intrinsic coercivity (H_{cj}) and magnetic induction coercivity (H_{cb}) as a function of LaPr-Co content for the M-type hexaferrite $Ca_{0.4}Sr_{0.6-x}(La_{0.8}Pr_{0.2})_xFe_{12-y}Co_yO_{19}$ magnets.

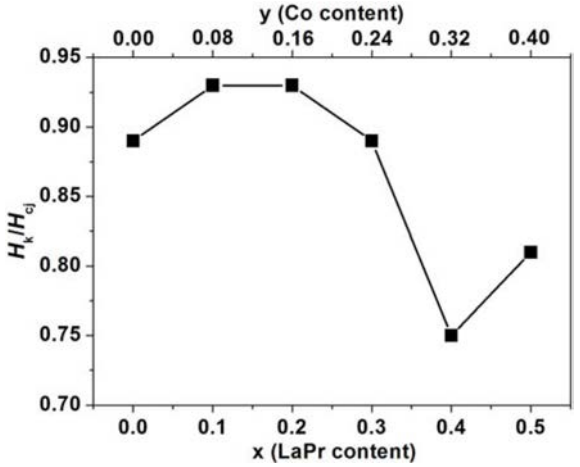

Fig. 8. The H_k/H_{cj} ratios as a function of LaPr-Co content for the M-type hexaferrite $Ca_{0.4}Sr_{0.6-x}(La_{0.8}Pr_{0.2})_xFe_{12-y}Co_yO_{19}$ magnets.

and 2a sites [28, 29]. In the LaPr-Co substituted M-type hexaferrites, in order to keep the electroneutrality, some Fe^{3+} ions will change into Fe^{2+} ions at 2a or $4f_2$ site. Thus, the decrease of remanence (B_r) with the increase of LaPr-Co content ($0.00 \le x \le 0.20$, $0.00 \le y \le 0.16$) can be attributed to increase in the number of Fe^{2+} ions on the 2a octahedral site. Some Fe^{3+} ($5\mu_B$) ions will change into Fe^{2+} ($4\mu_B$) ions at 2a site, which causes the magnetic dilution. The increase of remanence (B_r) with the increase of LaPr-Co content ($0.20 \le x \le 0.50$, $0.16 \le y \le 0.40$) can be explained by the site preference of Co^{2+} ($3.7\mu_B$) ions in the octahedral $4f_2$ sites. This decreases the negative magnetic moment of Fe^{3+} ions, and increases the whole magnetic moment, which leads to the increase of remanence (B_r).

The intrinsic coercivity (H_{cj}) and magnetic induction coercivity (H_{cb}) as a function of LaPr-Co content for the M-type hexaferrite $Ca_{0.4}Sr_{0.6-x}(La_{0.8}Pr_{0.2})_xFe_{12-y}Co_yO_{19}$ magnets are shown in Fig. 8. It is noted that H_{cj} increases with the increase of LaPr-Co content ($0.00 \le x \le 0.40$, $0.00 \le y \le 0.32$), and then decreases with increasing substitution content of LaPr ($0.40 \le x \le 0.50$) and Co ($0.32 \le y \le 0.40$). The coercivity of the ferrite magnets lies on the microstructure and magnetocrystalline anisotropy. The coercivity of the hexaferrites is expressed as the following equation [30]:

$$H_a = \alpha H_a - \frac{N(B_r + J_s^0)}{\mu_0} \quad (2)$$

where H_a represents the magnetocrystalline anisotropy field, N represents the grain demagnetization factor, J_s^0 represents the saturation polarization, and α represents the microstructure factor of the magnet. N can be regulated by the grain shape, and increase as the grain-shape is more platelet-shaped. α enlarges with the decrease of grain size, revealing the well-known H_c and grain size depency. The FE-SEM images shown in Fig. 4 exhibit that the grain size and grain morphology of the magnets remain unchanged with the increase of LaPr-Co content. So the values of N and α keep constant. For the low symmetry of crystal, the stronger uniaxial magnetic anisotropy of M-type hexaferrite is more sensitive to the low symmertry of trigonal bipyramidal site 2b [31]. Therefore, the increase of H_{cj} with the increase of LaPr-Co content ($0.00 \le x \le 0.40$, $0.00 \le y \le 0.32$) can be due to the following two factors. Firstly, the substitution of Sr^{2+} ($r = 1.180$ Å) ions by La^{3+} ($r = 1.061$ Å) and Pr^{3+} ($r = 1.013$ Å) ions results in greater lattice distortion, and the lower symmertry of trigonal bipyramidal 2b site, which leads to the increase of magnetocrystalline anisotropy [32]. Secondly, it has been reported that the magnetocrystalline anisotropy field increases with the increase of La-Co content (z) in the $Sr_{1-z}La_zFe_{12-z}Co_zO_{19}$ ($0 \le z \le 0.4$) hexaferrites [33]. The number of Fe^{2+} ions on the octahedral 2a site increases with the increase of LaPr-Co content. The Fe^{2+} ions can enhance the coercivity due to strong magnetocrystalline anisotropy of Fe^{2+} on 2a sites [34, 35]. For the magnetic powders containing LaPr ($x \ge 0.40$) and Co ($y \ge 0.32$), the decrease of H_{cj} with the increase of LaPr-Co content can be attributed to the below reason. The increase in the number of Co^{2+} ions at octahedral 2a site, increases with increasing LaPr-Co content, which will destroy the regular arrangement of the Fe^{3+} ions. This leads to the decrease of the magnetocrystalline anisotropy field. As seen from Fig. 6, for the magnetic powders with LaPr-Co content ($0.00 \le x \le 0.40$, $0.00 \le y \le 0.32$), the varying trend of H_{cb} is in agreement with that of H_{cj}, while for the magnetic powders with LaPr ($x \ge 0.40$) and Co ($y \ge 0.32$), the varying trend of H_{cb} is different from that of H_{cj}, H_{cj} decreases and H_{cb} increases. Fig. 8 shows the variation of H_k/H_{cj} ratios as a function of LaPr-Co content for the M-type hexaferrite $Ca_{0.4}Sr_{0.6-x}(La_{0.8}Pr_{0.2})_xFe_{12-y}Co_yO_{19}$ magnets. The H_k/H_{cj} ratio is one of the important indicators of the magnetic properties for the ferrite magnets, and could indicate the rectangularity of the demagnetizing curves for the magnets [36]. As seen

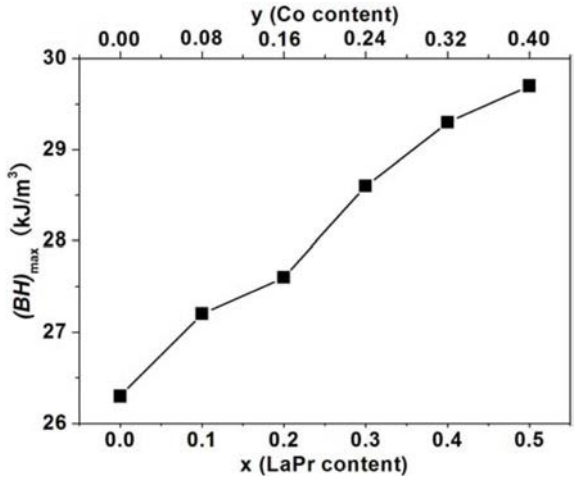

Fig. 9. The maximum energy product [(BH)max] as a function of LaPr-Co content for the M-type hexaferrite $Ca_{0.4}Sr_{0.6-x}(La_{0.8}Pr_{0.2})_xFe_{12-y}Co_yO_{19}$ magnets.

from Fig. 8, the H_k/H_{cj} ratio increases with the increase of LaPr-Co content ($0.00 \le x \le 0.10$, $0.00 \le y \le 0.08$), and keeps constant with the substitution content of LaPr ($0.10 \le x \le 0.20$) and Co ($0.08 \le y \le 0.16$), and then decreases with increasing substitution content of LaPr ($0.20 \le x \le 0.40$) and Co ($0.16 \le y \le 0.32$), while for the magnetic powders with LaPr ($x \ge 0.40$) and Co ($y \ge 0.32$), H_k/H_{cj} ratio increases. This should be the reason that the change of H_{cb} for the magnetic powders with LaPr ($x \ge 0.40$) and Co ($y \ge 0.32$) is different from that of H_{cj}.

Fig. 9 shows the variation of the maximum energy product [$(BH)_{max}$] as a function of LaPr-Co content for the M-type hexaferrite $Ca_{0.4}Sr_{0.6-x}(La_{0.8}Pr_{0.2})_xFe_{12-y}Co_yO_{19}$ magnets. The value of $(BH)_{max}$ increases with increasing LaPr-Co content. The maximum energy product is the maximum area in the second quadrant of the hysteresis loop, and thus the values of the remanence (B_r) and magnetic induction coercivity (H_{cb}) will have their influence on it. The changing trend of $(BH)_{max}$ for the hexaferrite $Ca_{0.4}Sr_{0.6-x}(La_{0.8}Pr_{0.2})_xFe_{12-y}Co_yO_{19}$ magnets is in agreement with that of the magnetic induction coercivity (H_{cb}) shown in Fig. 7.

Conclusions

The solid-state reaction method was used to synthesize a series of M-type hexaferrites with nominal composition of $Ca_{0.4}Sr_{0.6-x}(La_{0.8}Pr_{0.2})_xFe_{12-y}Co_yO_{19}$ ($0.00 \le x \le 0.50$, $0.00 \le y \le 0.40$). XRD patterns show that all the LaPr-Co substituted M-type hexaferrites are in single-phase with hexagonal structure and no impurity phase is observed in the structure. The FESEM images of the magnets show that the grains are hexagonal platelet-like, and the grain size of the magnets basically keeps unchanged with increasing LaPr-Co content.

The magnetic properties of the magnets were measured at room temperature by a permanent magnetic measuring system. B_r, first decreases, and reaches to the minimum value at $x = 0.20$, $y = 0.16$, and then increases with increasing substitution content of LaPr ($0.20 \le x \le 0.50$) and Co ($0.16 \le y \le 0.40$). H_{cj} increases with the increase of LaPr-Co content ($0.00 \le x \le 0.40$, $0.00 \le y \le 0.32$), and then decreases with increasing substitution content of LaPr ($0.40 \le x \le 0.50$) and Co ($0.32 \le y \le 0.40$). H_{cb} and $(BH)_{max}$ increase with increasing LaPr-Co content ($0.00 \le x \le 0.50$, $0.00 \le y \le 0.40$).

Acknowledgments

This work was supported by Scientific Research Fund of SiChuan Provincial Education Department (No. 14ZA0267 and No. 16ZA0330), the Major Project of Yibin City of China (No. 2016GY025), Scientific Research Key Project of Yibin University (No. 2015QD13) and the Open Research Fund of Computational Physics Key Laboratory of Sichuan Province, Yibin University (No. JSWL2015KFZ04). The Author K.M. Batoo is thankful to King Abdullah Isntitute For Nanotechnology, Deanship and Scientific Research, King Saud University for the financial support.

References

1. A. Goldman, Modern ferrite Technology, 2nd ed., Springer Science Inc., USA, 2006.
2. R.C. Pullar, Prog. Mater. Sci. 57 (2012) 1191-1334.
3. Y.J. Yang, F.H. Wang, J.X. Shao, D.H. Huang, X.S. Liu, S.J. Feng, C.E. Wen, J. Magn. Magn. Mater. 384 (2015) 64-69.
4. X. Liu, W. Zhong, S. Yang, Z. Yu, B. Gu, Y. Du, J. Magn. Magn. Mater. 238 (2002) 207-214.
5. R. Ezhil Vizhi, V. Harikrishnan, P. Saravanan, D. Rajan Bahu, J. Cryst. Growth 452 (2016) 117-124.
6. J.F. Wang, C.B. Ponton, I.R. Harris, J. Alloys Compd. 403 (2005) 104-109.
7. L.N. Pan, F.M. Gu, D.R. Cao, P.P. Jing, J.N. Li, J.B. Wang, Q.F. Liu, Appl. Phys. A, 122 (2016) 583.
8. B.H. Bhat, B. Want, Appl. Phys. A 122 (2016) 148.
9. L. Lechevallier, J.M. Le Breton, A. Morel, J. Teillet, J. Alloys Compd. 359 (2003) 310-314.
10. A. Sharbati, J. Mola, V. Khani, J. Mater. Sci.: Mater. Electron. 68 (2000) 182-185.
11. D.A. Vinnik, A.S. Semisalova, L.S. Mashkovtseva, A.K. Yakushechkina, S. Nemrava, S.A. Gudkova, D.A. Zherebtsov, N.S. Perov, L.I. Isaenko, R. Niewa, Mater. Chem. Phys. 163 (2015) 416-420.
12. A. Awadallah, S.H. Mahmood, Y. Maswadeh, I. Bsoul, M. Awawdeh, Q.I. Mohaidat, H. Juwhari, Mater. Res. Bull. 74 (2016) 192-201.
13. Y.J. Yang, F.H. Wang, X.S.Liu, J.X. Shao, S.J. Feng, D.H. Huang, M.L. Li, J. Magn. Magn. Mater. 422 (2017) 209-215.
14. Y.J. Yang, F.H. Wang, J.X. Shao, X.S.Liu, D.H. Huang, J. Ceram. Soc. JPN. 125 (2017) 27-31.
15. Y.J. Yang, F.H. Wang, X.S. Liu, J.X. Shao, D.H. Huang, J. Magn. Magn. Mater. 421 (2017) 349-354.
16. P. Sharma, R.A. Rocha, S.N. de Medeiros, B. Hallouche,

A. Paesano Jr, J. Magn. Magn. Mater. 316 (2007) 29-33.
17. X.Q. Shen, M.Q. Liu, F.Z. Song, Appl. Phys. A 104 (2011) 109-116.
18. Y.J. Yang, X.S. Liu, D.L. Jin, Y.Q. Ma, Mater. Res. Bull. 59 (2014) 37-41.
19. Y.J. Yang, X.S. Liu, Mater. Technol. 29 (2014) 232-236.
20. Y.M. Kang, Y.H. Kwon, M.H. Kim, D.Y. Lee, J. Magn. Magn. Mater. 382 (2015) 10-14.
21. M.J. Iqbal, S. Farooq, J. Alloys Compd. 505 (2010) 560-567.
22. Z.F. Zi, Q.C. Liu, J.M. Dai, Y.P. Sun, Solid State Commun. 152 (2012) 894-897.
23. H.M. Khan, M.U. Islam, Y.B. Xu, M.N. Ashiq, I. Ali, M.A. Iqbal, M. Ishaque, Ceram. Int. 40 (2014) 6487-6493.
24. H.M. Khan, M.U. Islam, Y.B. Xu, M.A. Iqbal, I. Ali, J. Alloys Compd. 589 (2014) 258-262.
25. R.R. Bhosale, R.S. Barkule, D.R. Shengule, K.M. Jadhav, J. Mater. Sci.: Mater. Electron. 24 (2013) 3101-3107.
26. M.J. Iqbal, B.ul-Ain, Mater. Sci. Eng. B 164 (2009) 6-11.
27. T.R. Wagner, J. Solid. State Chem. 136 (1998) 120-124.
28. L. Lechevallier, J.M. Le Breton, J. Teillet, A. Morel. F. kools, P. Tenaud, Physica B 327 (2003) 135-139.
29. J.M. Le Breton, J. Teillet, G. Wiesinger, A. Morel. F. kools, P. Tenaud, IEEE Trans. Magn. 38 (2002) 2952-2954.
30. F. Kools, A. Morel, R. Grössinger, J.M. Le Breton, P. Tenaud, J. Magn. Magn. Mater. 242-245 (2002) 1270-1276.
31. R.C. Pullar, Prog. Mater. Sci. 57 (2012) 1191-1334.
32. I. Bsoula, S.H. Mahmoodb, A.F. Lehloohc, A. Al-Jamela, J. Alloys Compd. 551 (2013) 490-495.
33. G. Asti, F. Bolzoni, J.M. Le Breton, M. Ghidini, A. Morel, M. Solzi, F. Kools, P. Tenaud, J. Magn. Magn. Mater. 272-276 (2004) e1845-e1846.
34. C.J. Li, B. Wang, J.N. Wang, J. Magn. Magn. Mater. 324 (2012) 1305-1311.
35. S. Qunnunkad, Solid State Commun. 138 (2006) 472-475.
36. Z.M. Wang, Ferrite Production Technology, Chongqing University Press, Chongqing, 2013.